




Ultra-sensitive probe of spectral line structure and detection of isotopic oxygen

Richard M. Garner^{1,3} · A. N. Dharamsi² · M. Amir Khan¹ 

Received: 9 August 2017 / Accepted: 16 December 2017 / Published online: 26 December 2017
© Springer-Verlag GmbH Germany, part of Springer Nature 2017

Abstract

We discuss a new method of investigating and obtaining quantitative behavior of higher harmonic ($> 2f$) wavelength modulation spectroscopy (WMS) based on the signal structure. It is shown that the spectral structure of higher harmonic WMS signals, quantified by the number of zero crossings and turnings points, can have increased sensitivity to ambient conditions or line-broadening effects from changes in temperature, pressure, or optical depth. The structure of WMS signals, characterized by combinations of signal magnitude and spectral locations of turning points and zero crossings, provides a unique scale that quantifies lineshape parameters and, thus, useful in optimization of measurements obtained from multi-harmonic WMS signals. We demonstrate this by detecting weaker rotational–vibrational transitions of isotopic atmospheric oxygen ($^{16}\text{O}^{18}\text{O}$) in the near-infrared region where higher harmonic WMS signals are more sensitive contrary to their signal-to-noise ratio considerations. The proposed approach based on spectral structure provides the ability to investigate and quantify signals not only at linecenter but also in the wing region of the absorption profile. This formulation is particularly useful in tunable diode laser spectroscopy and ultra-precision laser-based sensors where absorption signal profile carries information of quantities of interest, e.g., concentration, velocity, or gas collision dynamics, etc.

1 Introduction

In a typical absorption experiment, the absorption coefficient is obtained from the absorbed intensity, dI , over a length dz . The standard relation describing the absorption signal or the attenuation of intensity in an infinitesimal pathlength dz is given by $dI = e^{-\alpha^{(v)}} I dz$, where α is the absorption coefficient (m^{-1}) or the optical depth. It is the signal contrast from a reference that gives information about the parameter being measured. Therefore, in a conventional absorption spectroscopy, measurements are based on changes in the photon intensity with respect to a reference. In most cases these measurements are performed to retrieve absolute abundances of gas species, as with tunable diode laser sensors. Therefore, in many diode laser spectroscopy measurements

the peak absorption (linecenter) provides information about the density (or concentration) or the environment of the gas, e.g., temperature or pressure. An early example of this was high-resolution line-broadening and collisional measurements of carbon dioxide bands [1, 2], where the linecenter magnitude shows a characteristic saturation behavior as the pressure (at fixed temperature) is increased. Such measurements are quite important since the absorption signal power is the maximum at the peak value, and its variations can reveal the nature of collision dynamics [1–4]. Therefore, in many instances, measurements at linecenter are quite adequate.

In many gas-sensing applications [5–7], fitting of the experimental spectra with a known gas standard as a reference is also commonly used for absolute values of the gas concentration. Therefore, value of the absolute abundance can be obtained either with measurements performed at the linecenter, or across the full line spectrum by the spectral fitting (with respect to a reference gas spectrum) of the absorption profile. However, because such measurements of the absorption signal are performed either at one wavelength (at linecenter) or considering only the cumulative absorption signal power of the individual line spectrum, they do not reveal the complete picture. In particular, subtle

✉ M. Amir Khan
mkhan@desu.edu

¹ Department of Physics and Engineering Physics, Delaware State University, Dover, DE 19901, USA

² Department of Electrical and Computer Engineering, Old Dominion University, Norfolk, VA 23529, USA

³ Present Address: Department of Aerospace Engineering, Kansas State University, Manhattan, KS 66506, USA

perturbations in the lineshape profile will not be apparent in the spectral fitting analysis, or in the magnitude of the linecenter or its variation with respect to a parameter, such as pressure or temperature.

In this paper, we illustrate that spectral features not only around the linecenter are important, often features in the wing of the lineshape profile may be more sensitive to subtle effects. For our purposes, the wing region is the spectral location greater than one linewidth from the linecenter. Therefore, sensitivity of laser-based trace gas sensors is directly correlated with signal contrast with the background from several sources including DC baselines and slopes from residual amplitude modulation (RAM) effects, fringe or scattering from optical elements, and, more importantly, interference from neighboring line transitions in a congested overlapping line spectrum. Such quantitative metrics are necessary for ultra-precision laser-based sensors and sensing systems that primarily rely on sensitive measurements of gas species based on lineprofiles and resultant absorption signals to retrieve gas concentration or mixing ratios, or quantify gas molecular collision dynamics to obtain relevant optical transition matrix element. Therefore, for ultra-sensitive precision measurements, it is important to investigate the complete structure of the signal both around the linecenter and in the wing region of the profile because certain regions of the lineshape profile could be more sensitive to subtle changes than the regions where the signal is maximal.

Wavelength modulation spectroscopy (WMS) has long been used [8–13] as a tool to perform sensitive measurements in trace gas detection and tunable diode laser sensors. The technique involves modulation of a laser, tuned to a spectral feature of interest, which probes a sample

gas in a media. The modulated absorption signal obtained on a photodetector is demodulated at various integral (N) multiple of the fundamental frequency. This is commonly achieved by a lock-in amplifier where the signal obtained can be expressed as a Fourier component or N th Fourier harmonic of the modulated absorption signal. Therefore, commonly used $2f$ -WMS detection (for $N=2$) corresponds to demodulation at twice the fundamental frequency. In many WMS schemes detection at $N>2$ are also investigated. In particular, it has been shown [9, 12, 13] that detection at higher harmonics often reveals structure in the absorption region not otherwise seen at lower harmonics. The synchronous phase-sensitive WMS technique [8, 12–17] provides a probe that depicts variations of the lineshape function. These variations correspond, approximately, to the derivatives of the lineprofile. WMS signals with synchronous detection at the N th harmonic of the modulation frequency (Nf detection) yield $N+1$ turning points and N zero crossings. These $2N+1$ salient features (and their combinations) contain a large fraction of information of the lineshape characteristics and, hence, of the molecular collision dynamics. We refer these salient features as ‘markers’ because they provide an easily identifiable marker for a location within the spectra to make a measurement across a lineprofile. Owing to its derivative-like features, the turning points and zero crossings of a WMS signal provide key markers throughout the spectrum of the lineshape profile. Figure 1a and b shows $2f$, $4f$, $3f$ and $5f$ signals normalized to the direct absorption signal where the turning points (or zero crossings) are distributed across the spectrum. In a typical WMS measurement the locations of these salient points can be controlled by suitable choice of experimental parameters.

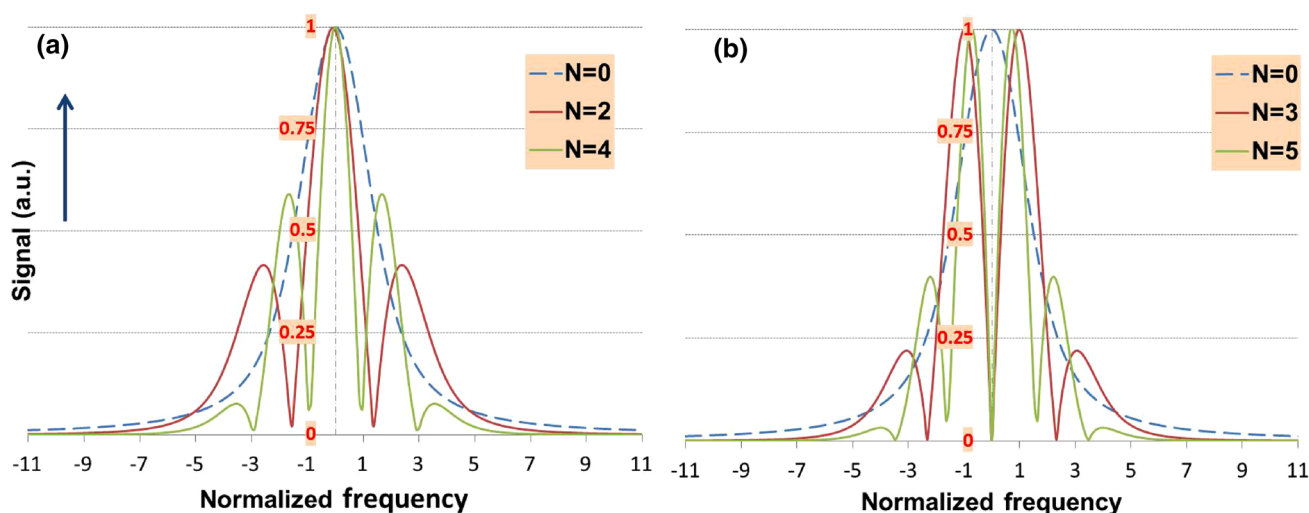


Fig. 1 Theoretical models of direct absorption (dashed) and higher harmonic WMS profiles scaled to unity with the x -axis normalized to the linewidth value—indicating distance in linewidths from the

linecenter. For various, even (a) and odd (b) WMS detection orders ($N=2$ – 5) zero crossing and turning points span across the direct absorption profile

In this paper, we discuss techniques that probe the full structure of the lineshape profile enabled by wavelength modulation spectroscopy (WMS). In addition, we quantify complexity in structure and sensitivity to parameters such as temperature, pressure and optical pathlength across the full lineprofile including the far-wing region. This is achieved by quantifying variations in the signal at turning points and zero crossings of a WMS signal based on sensitivity to environmental conditions and lineprofile parameters. We utilize this key aspect as an advantage of higher harmonic WMS detection. In particular, we demonstrate higher order WMS as a quantitative metric that embodies characteristic behavior in the wing region. We show that simultaneously investigating multi-harmonics of the absorption signal provides a multi-faceted (or multi-dimensional) approach to spectroscopic measurements. We also show that a signal that provides greater contrast from point to point in phase-space is easier to measure, even when it may not exhibit the greatest cumulative signal-to-noise ratio (SNR). In such cases, conventional SNR is not the most suitable metric for optimizing the measurement, especially when quantifying sensitivity to parameters such as temperature, pressure or spectral line resolution. A significant enhancement in signal contrast may occur as a consequence of greater structure leading to greater sensitivity of higher harmonic WMS signals even though the fractional change in the direct absorption signal magnitude is limited by experimental SNR. This is demonstrated by the detection and resolution of weaker transitions of isotopic oxygen— $^{16}\text{O}^{18}\text{O}$ —using higher harmonic WMS.

We conceptualize the notion of structure as spectral locations and signal magnitude of individual turning points and zero crossings (with respect to the linecenter) as a metric of measurements. Therefore, in this paper we study the relationship between turning points and zero crossings and their dependence on lineshape parameters. A turning point in the N f-WMS signal (i.e., N th harmonic detection) generally corresponds to a zero crossing in the $(N+1)$ f-WMS signal, since an N f-WMS signal resembles the N th frequency derivative-like features of the lineshape function. The signal magnitude and spectral locations of these features depend on the experimental parameters such as the frequency modulation index, amplitude modulation, sample length, as well as on the lineshape function and the oscillator-strength of transition being probed. The span of zero crossings and turning points provides key markers at various locations throughout the spectrum as shown in Fig. 1. Furthermore, detection at higher harmonics provides a greater number of such markers. The relative spectral spacing between zero crossings and turning points and their span (from the linecenter into the wings) all depend strongly on the experimental controls of WMS. In the following sections we provide a quantitative description of the WMS signal structure, the importance of zero crossings and turning points in higher harmonic

detection, and quantify information in the wing region of the absorption profile. For the analysis we consider a Voigt lineshape profile and demonstrate sensitivity of higher harmonic detection with parameters such as temperature, pressure and optical depth. As an example we probe several rotational–vibrational molecular, atmospheric oxygen transitions of $^{16}\text{O}_2$ and $^{16}\text{O}^{18}\text{O}$ in the A-band.

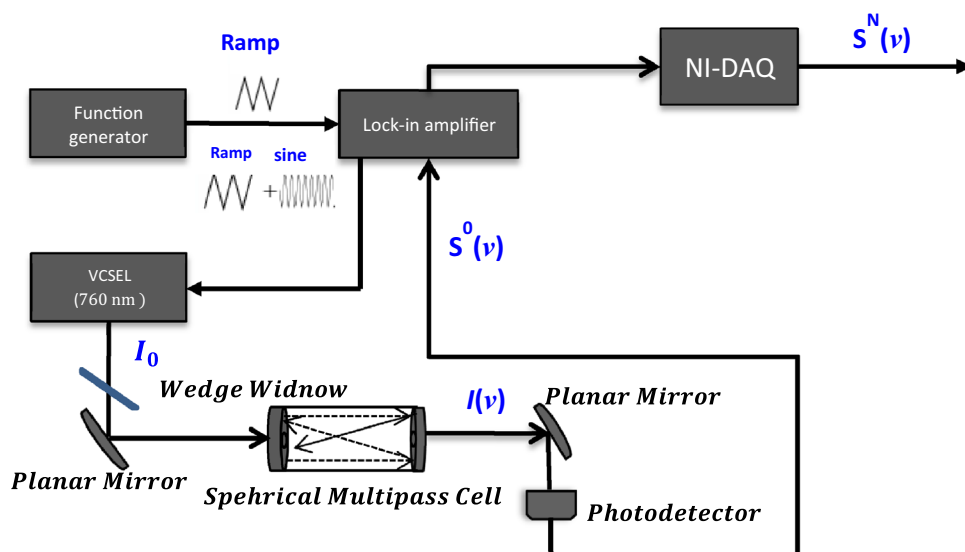
2 WMS structure and higher harmonic detection (HHD)

In this section, we illustrate experimental procedure and WMS measurements of atmospheric oxygen transitions in 760 nm region. A methodology of spectral fitting is obtained by simultaneously using multiple WMS detection orders, i.e., by performing WMS detection from $N=1$ to $N=8$ and fitting experimental spectra with theoretical models based on HITRAN parameters. Due to significant variations in signal magnitude from linecenter to wing region, residuals alone are not suitable measure of a fit. Therefore, fractional errors across the spectrum and its standard deviation for a particular WMS detection are used to quantify fit between experiments and theory, or determine uncertainty in experimentally measured parameters. The concept of structure is elucidated in higher harmonic WMS signals where sensitivity to a parameter, e.g., linewidths (i.e., temperature or pressure) is characteristic of zero crossing and turning points. The sensitivity and interplay of signal structure are demonstrated by probing atmospheric oxygen A-band rotational–vibrational transitions at 760 nm. This band includes combination of the strong and weak transition of oxygen $^{16}\text{O}_2$ (e.g., RR(13,13) transition) and its isotopes including $^{16}\text{O}^{18}\text{O}$ transitions.

2.1 Experimental procedure

The experimental setup as shown in Fig. 2 involves a single-mode continuous wave tunable diode vertical cavity surface emitting laser (VCSEL) operating at 760 nm wavelength (ULM—Philips Photonics). The laser was operated by a laser diode current driver and temperature controller (Newport-6100). The laser current is modulated to probe several atmospheric broadened oxygen line transitions in the range of 760.30–760.40 nm. The ramp signal generated by the function generator produces slow scan of the laser current (200 Hz) which is added to a fast sinusoidal modulation (10 KHz) produced internally by the lock-in amplifier (Zurich Instrument HF-2LI). The collimated laser beam is channeled into the optical multipass cell using combination of planar mirrors and wedge windows to counter Fabry–Perot fringing or back-reflection effects. The multipass cell was based on Heriot cell design [18] to achieve variable pathlength

Fig. 2 Schematic of the experimental setup. The probe VCSEL samples the atmospheric oxygen in the wavelength region of 760 nm at room temperature



in the range of 88–210 m. A set of 3-inch dielectric-coated astigmatic concave mirrors were used for the multipass cell in open-path configuration. The modulated absorption signal [$S^0(\nu)$] at the detector (Teledyne Judson Technologies) is demodulated at various integral frequencies of the fundamental modulation frequency (ω_m) using a lock-in amplifier. The Nf -WMS signal [$S^N(\nu)$] is obtained on the lock-in amplifier [19, 20]. Therefore, a probe, modulated at modulation frequency, ω_m with modulation amplitude (β in Hz, i.e., spectral span in the laser frequency due to amplitude of the sinusoidal signal), can be expressed as $I(\nu + \beta \cos[\omega_m t])$. In the experimental procedure, the modulated laser beam is swept slowly across the absorption feature by a slow ramp signal.

2.2 Theoretical description of WMS signals

The effective normalized (modulated) absorption signal recorded by the detector is, therefore,

$$\frac{\Delta I(\nu + \beta \cos(\omega_m t))}{I_0} = 1 - \exp\{-n\bar{\sigma}Lg(\nu + \beta \cos(\omega_m t))\} \tag{1}$$

Using absorption lineshape function as a Voigt lineshape profile [12] is given by the equation:

$$g(x) = \frac{b^2}{\pi^{3/2}\delta\nu_L} \int_{-\infty}^{\infty} dt \frac{e^{-t^2}}{(x-t)^2 + b^2} \tag{2}$$

Therefore, a modulated absorption signal due to Voigt lineshape profile is given by

$$g\left(x + m \cos \theta, \overline{\delta\nu_D}\right) = \frac{1}{\pi^{3/2}} \frac{b}{\overline{\delta\nu_D}} \int_{-\infty}^{\infty} dt \frac{e^{-t^2}}{(x + m \cos \theta - t)^2 + b^2} \tag{3}$$

where n is the number density of molecules, $\bar{\sigma}$ is the integrated absorption cross section and L is the pathlength. The linewidth parameter is defined as ratio of collision half-width with normalized Doppler half-width, $b = \delta\nu_L/\overline{\delta\nu_D}$, where $\overline{\delta\nu_D} = \nu_0 \left(\frac{2kT \ln 2}{Mc^2}\right)^{1/2} = \frac{\delta\nu_D}{2(4 \ln 2)^{1/2}}$.

Also, in Eqs. (2) and (3), x is the normalized frequency, $x \equiv (\nu - \nu_0)/\overline{\delta\nu_D}$, and m is the frequency modulation index defined by $m = \beta/\overline{\delta\nu_D}$, β is the modulation amplitude in Hz and $\theta = \omega_m t$.

Expanding the above signal given by Eq. (1) in a Fourier series to express the N th harmonic signal [8] one obtains the corresponding N th order WMS (or Nf) signal, S^N . Without considering weak absorption approximation, the mathematical form of Nf -WMS signal is given by the Eqs. (4) and (5):

$$S_N(x) = \frac{I_0}{\pi} \int_{-\pi}^{+\pi} d\theta \Delta I(x + m \cos \theta) \cos(N\theta) d\theta \tag{4}$$

Therefore, for a Voigt lineshape profile, the N th order WMS signals is given by

$$S^N(x) = \frac{I_0}{\pi} \int_{-\pi}^{\pi} d\theta \left[1 - \exp\left(\frac{n\bar{\sigma}L}{\pi^{3/2}} \frac{b}{\overline{\delta\nu_D}} \left\{ \int_{-\infty}^{\infty} dt \frac{e^{-t^2}}{(x + m \cos \theta - t)^2 + b^2} \right\} \right) \cos(N\theta) \right] \tag{5}$$

(a) *Structure in WMS-HHD:* Fig. 3a and b shows experimental and modeled 2f- and 6f-WMS signals of oxygen A-band RR(13,13) rotational–vibrational transitions centered at 760.378 nm (13151.34015 cm^{-1}) with air-broadened

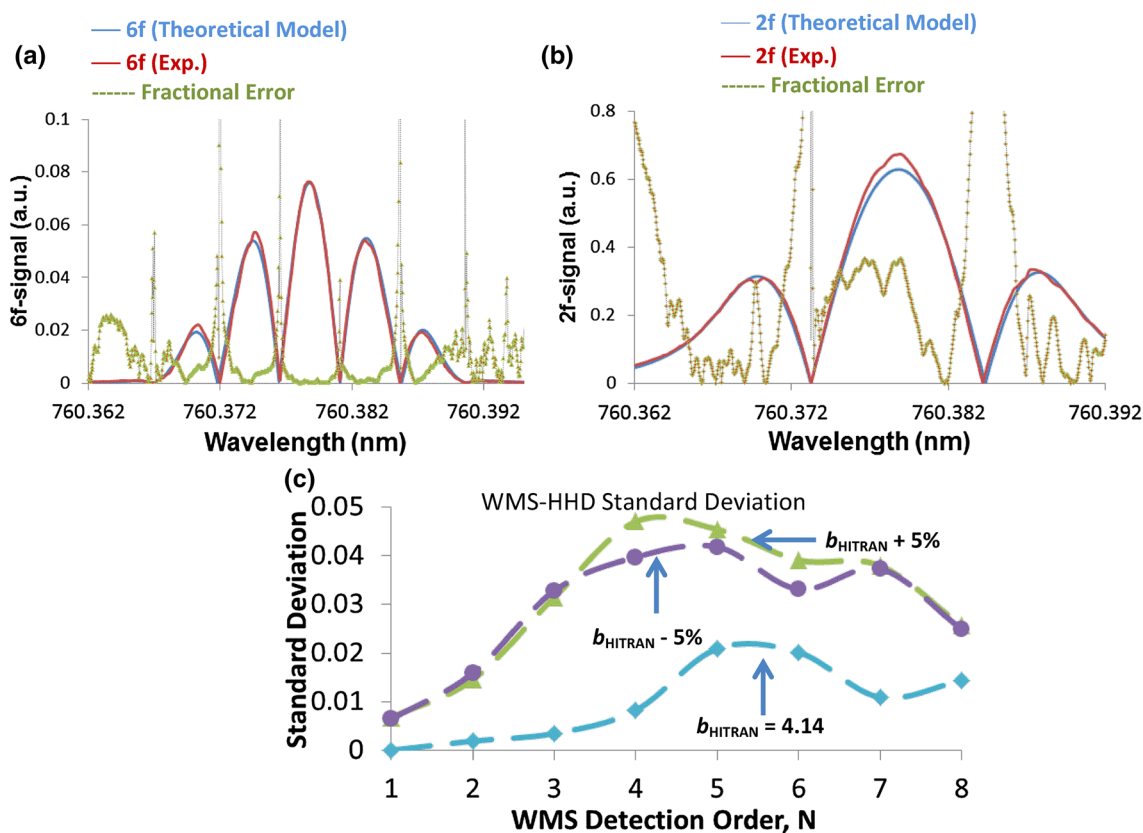


Fig. 3 Experimental and theoretical signal (corresponding to $b_{\text{HITRAN}}=4.14$) of 2f-WMS (a) and 6f-WMS (b) detection of atmospheric oxygen $^{16}\text{O}_2\text{-RR}(13,13)$ line transitions. Fractional errors is

imposed in a and b. In c the standard deviation of fractional errors was estimated for 5% uncertainty in the b parameter at various detection orders

collision half-width of 0.046 cm^{-1} according to the HITRAN 2017 database [21]. The experimental WMS-HHD spectra were obtained by scanning the modulated VCSEL in the wavelength range of 760.30–760.40 nm, and demodulating the absorption signal at frequencies that are integral multiple of fundamental modulation frequency. The experimental spectra are recorded on a data-acquisition card (NI-DAQ USB 6211). The experimental SNR of a given WMS (N th) detection order is obtained from the ratio of signal peak values and the average noise floor (from the spectral region where there is no absorption).

The models and fit are generated using built-in Matlab algorithms in LabVIEW; both are implemented in the DAQ. The model uses air-broadened collision full-width at half maximum (FWHM) of $\delta\nu_L=2.76\text{ GHz}$ given in the HITRAN [21] database, and the Doppler width was estimated to $\delta\nu_D=0.669\text{ GHz}$ at room temperature. Therefore, the linewidth parameter, b (ratio of collision and Doppler widths), using HITRAN values of collision width was estimated to be $b=4.14$. The fitting was done assuming a Voigt lineshape function and uncertainty in ambient conditions resulting in b values of $b\pm 5\%$. The scatter plots imposed on 2f and 6f models in Fig. 3a and b show the fractional errors

between theory ($b=4.14$) and experiment across the full-spectral profile. The fractional errors are defined as

$$E^N(x) \equiv \left| \left(\frac{s^N(x)_{\text{WMS Model}}}{s^N(x)_{\text{WMS Experiment}}} \right) - 1 \right| \quad (6)$$

In our analysis we compared theoretical models and experimental data of various N f-WMS signals to investigate the spread of fractional errors across the spectrum, and standard deviation of each WMS detection order. The mismatch occurs due to differences in experimental and theoretical values of N f signals resulting from a fitting parameter, e.g., b , in this case. In our analysis the theoretical model is the one that best fits the experiment when the standard deviation of fractional errors is least for a set of b parameters. These values of b parameter, obtained from fits may show deviations from HITRAN values. It is noted that HITRAN values are continuously improved based on high-precision experimental data from measurements. Therefore, WMS-HHD technique presented above could improve on values provided in the HITRAN database. In addition, modeling at several WMS-HHD spectra simultaneously provides a multi-dimensional approach and higher set of stringent constraints in fitting routines. In other words for each value of b

parameter, there are eight simultaneous measurements and theoretical models for $N=1\text{f}$ – 8f WMS detection.

From Fig. 3a and b, which shows 2f and 6f (corresponding to $N=2$ and $N=6$) signals, it is clear that mismatches are greater at the locations of zero crossings and turning points. Higher detection orders with greater number of zero crossings and turning points show enhanced spectral mismatch and scatter of fractional errors. It is seen that a particular b value, which is optimal (i.e., lowest standard deviation) for a particular detection order may not be optimal for another detection order. This aspect is illustrated in Fig. 3c, which shows various $N\text{f}$ -standard deviations of fractional errors of 1f to 8f WMS-HHD due to uncertainty in the b parameter. Therefore, standard deviations can be regarded as cumulative figures of merit for a particular WMS detection order. An “ideal” fit between theory and experiment will have a constant value of fractional error (or zero standard deviation) throughout the spectrum. However, for the same uncertainty in the b parameter, and specific WMS-SNR limitations, the signal with the greater structure, i.e., various higher detection orders will produce a higher mismatch or standard deviation. Further, it is also noted that even though 8f detection can result in greater structure, its usability is limited by the SNR. It is seen that fractional error, which is greater in the wing region, is ultimately limited by the SNR of the measurement. The SNR criteria are chosen based on experimental spectra by identifying ratios of signal peak (at the linecenter for even-harmonics and maximal turning point for odd-harmonics) and noise floor (value of signal in spectral regions when there is no absorption—in far-wing regions). It is noted that we only considered the span of the spectral region where the cumulative SNR was greater than 5 for all WMS-HHD and values of fractional error does not exceed 50%, to avoid extremely high values of fractional errors due to low values of experimental signal. The SNR criteria will essentially eliminate values that are close to zero that would have potentially resulted in extremely large values of fractional errors, therefore, biasing the standard deviation values to higher magnitudes. Therefore, any data point whether it is around region of zero crossings or in the wing region will not produce an outsized weighting of such regions. This is seen as lower values of the standard deviation at 8f than at 6f in Fig. 3c.

Further, it is the standard deviation of this type—between an experiment and a model—with a particular parameter such as the linewidth that ultimately allows the precision of a measurement to be improved: the greater the value of standard deviation that occurs as a result of a fixed change in an assumed value, the more precise the measurement will be when the standard deviation is minimized, further constraining the b parameter. Hence, all other factors being the same, Fig. 3c shows that under the specified SNR conditions, 4f and 5f detection is more suitable for optimization

and correction for errors and ultimately facilitates the most precise results in our experiment. Further, it is noted that the value of standard deviation of a direct absorption signal would be minimal because of the absence of significant structure in the signal profile. By “direct” absorption we mean the absorption signal such as that obtained by conventional spectroscopy using no probe modulation but with the laser probe still being swept slowly across the absorption line. Such direct absorption signals may be viewed as a subset, with $N=0$, of WMS signals.

(b) Structure in the line-wing region and spectral fitting: Another approach to investigate uncertainty in linewidth parameter is standard deviation in segmented regions of WMS signal. In this, the standard deviation is considered within each segment of the WMS spectra with regions between the two consecutive zero crossings. For example, in an even-harmonic WMS signal the first segment is the region around the linecenter, approximately between zero crossing on positive and negative values of the normalized frequency (i.e., $x = \pm 1$). This is illustrated in Fig. 4, where theoretical and experimental 6f and 2f spectra are shown along with their respective fractional errors across the spectrum in Fig. 4a and b. The normalized frequency scale in Fig. 4a and b can be converted into segments, where each segment indicated in Fig. 4c covers a range of normalized frequencies across the spectrum. For example, for 6f the range $-1 < x < +1$ is referred to Region-0, similarly, range $+1 < x < +2$ is Region-1. Also, for 2f signal the range $-2 < x < +2$ is Region-0, and $+2 < x < +5$ is Region-1. In other words, in Fig. 4c segmented Regions (the x -axis) indicated as Region-0 is the span of one linewidth around the linecenter or normalized frequency, $x=0$, similarly, Region-1 indicates one linewidth span between the first and second zero crossing from $x=0$, and Region-2 indicates one linewidth span between second and third zero crossing from $x=0$. The standard deviation is investigated in each segment where zero crossings and turning points provide ability to visually discriminate regions in a quantifiable metric, as seen in Fig. 4c. To illustrate our methodology Fig. 4c suggests wing region of the lineprofile is more sensitive to measurements, which will not be apparent in lower detection order, e.g., 2f. Here again, WMS-HHD signals, e.g., 4f and 6f show higher magnitudes of standard deviations, which differ from one region to another and provide tools to quantify changes in the lineprofile. The line-wing regions ($|x| > 1$) of WMS-HHD signals are unique and turning points in the wing region can provide suitable probe markers in this region.

It could be generalized that the sensitivity of turning points due to uncertainty in linewidth parameter, or sensitivity due to signal perturbation from changes in environmental conditions—shown in later sections—is characteristic of the lineshape profile and exemplifies nature of profile slopes in the wing region. Therefore, two key points are highlighted

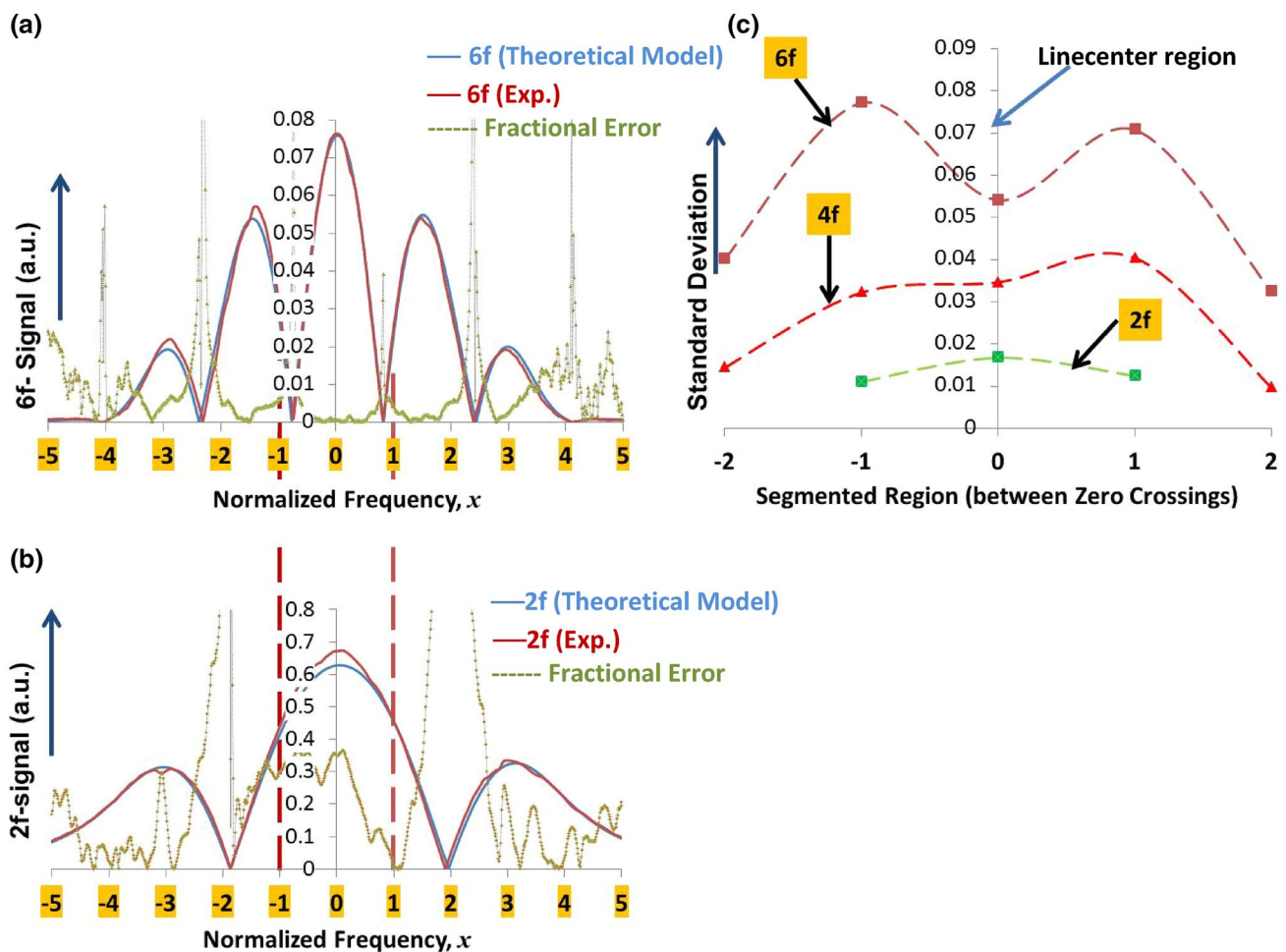


Fig. 4 Experimental and theoretical 2f- (a) and 6f-WMS (b) spectra of atmospheric oxygen $^{16}\text{O}_2\text{-RR}(13,13)$ line transitions. Fractional errors due to uncertainty in linewidth parameter, b , is shown for both

2f and 6f-WMS spectra. Standard deviation of errors (c) in segmented regions is shown as quantitative measure of sensitivity around linecenter and in the wing region of the profile

while considering WMS-HHD signals: (a) within the limitations of SNR, higher order detection provides more structure suitable for optimizing the experiment, and (b) in certain situations, line-wing region can be more sensitive to certain lineprofile deviations than regions around the linecenter. In addition, WMS-HHD signal structure also reveals distinct physical features that are otherwise obscure in physical changes in the environment resulting from line-broadening mechanisms or changes in pressures and optical depth in an experiment. This is described in the following sections.

To demonstrate sensitivity of WMS-HHD signals with changes in environmental conditions and implications of signal structure, we consider changes from a known reference signal at atmospheric pressure or temperature. Experimental controls such as the modulation index play a key role in determining the WMS- N f signal magnitude and sensitivity to any variations in the lineshape profile. The spectral spacing between zero crossings and turning points and their span (from the linecenter into the wings) depends strongly on the

frequency modulation index, which can be optimized to control locations of turning points and zero crossing in the wing region. For example, to resolve overlapping lines [12, 13, 22–26] a frequency modulation index of the order of the line separation is most suitable. This is because the probe laser effectively samples the spectral region of the direct absorption signal in the range of the spectral swing of the modulation. Similarly, in optical pathlength saturation effects [22, 26], where the signal broadens due to strong absorption around the linecenter, the effects are most easily discernible when the frequency modulation index is comparable to the spectral span of such broadening in the direct absorption signal. Any perturbation or deviation in the lineshape profile is strongly manifested in the wing region (because the absorption in those regions is smaller compared to that around the linecenter) and it is quite conceivable that a small change in the gas dynamics can produce significant change in the wings. Since WMS signals are an effective representation of the N th derivative of the absorption signal, such

features in the wings provide sensitive locations with which to probe any perturbations or deviations in an assumed line-shape profile.

Finally, it is emphasized that zero crossings and turning points serve as key indefinable locations in the spectrum where effects of line-broadening uncertainties are enhanced. Therefore, in a WMS-HHD signal instead of analyzing the full spectrum, turning points can be used as a unique metric of signal structure. In the following section we will investigate the sensitivity of turning points of various WMS-HHD signals under variable physical conditions like changes in temperature or pressure from a reference. Therefore, now the sensitivity will be estimated based on fractional changes in turning points between the reference and perturbed WMS-HHD signal. This approach can provide unique calibration schemes of sensor systems and fast signal processing while maintaining full sensitivity of the spectral profile.

3 Sensitivity to line-broadening mechanisms in the line-wing region

Spectral lineprofiles show characteristics of broadening mechanisms, namely collisions and Doppler broadening or their combination. In many field-based trace gas sensors measurements could significantly be affected by changes in the environment requiring frequent sensor calibrations. This could even be more relevant for open-path sensors where the sample and the probe laser-sensor are fully exposed to the environment. In such situations it is highly required to monitor lineshape behavior with fluctuations in pressure or temperature. This could certainly be achieved by introducing additional temperature or pressure probes; however, using WMS-HHD features or tracking behavior of turning points, a direct and synchronous measurement of such changes in the environment could be attained in real time. It is known that Doppler profiles are broader around the linecenter, whereas, collision-broadened profiles are narrower with steep slopes in the wing region. This characteristic behavior is further enhanced in the sensitivity of turning points of WMS-HHD signals when temperature or pressure is changed. A comparison of profile variations in terms of percentage change in turning points of WMS-HHD signals and linewidth sensitivity is shown using theoretical models and experimental datasets. We considered two cases of pure Doppler and collision broadening by changes in pressure and temperature, and analyzed the signal structure of WMS-HHD specifically focusing on the variation in turning points. We show that WMS-HHD signals and their signal magnitudes (at the linecenter and at turning points across the spectrum) are more sensitive to collision-broadened profiles than Doppler-broadened profiles, as seen in Fig. 5.

3.1 Structure and sensitivity to Doppler and collision broadening in the line-wing region

Figure 5a shows linecenter values of a direct absorption signal due to variation in collision and Doppler widths. We considered a Voigt lineshape profile of a reference signal with a linewidth parameter resulting from equal contribution from Doppler and collision broadening mechanisms. Therefore, the variation in signal magnitudes is estimated with respect to a signal with linewidth parameter, $b = 1$, i.e., when the collision and Doppler widths are equal. The variation in the b parameter was modeled with $\pm 10\%$ changes. It has been shown previously [23–26] that the linecenter magnitude of WMS-HHD signal is sensitive to the line parameter [23, 24, 27]; however, there is limited understanding on the characteristic behavior of the signal with the broadening mechanisms. Figure 5c and d show the percentage changes in the first, second, and third turning points covering the full spectral span of a typical 5f-WMS signal (Fig. 5a) due to two different broadening mechanisms. Comparing the Doppler and collisional broadening mechanisms by investigating the linecenter (in direct absorption) in Fig. 5a, or turning points of WMS-HHD signals in Fig. 5c and d, the turning points show higher sensitivity to collision broadening (or pressure) than the Doppler broadening (or temperature) effects. This could be an important tool to investigate high-precision temperature- and pressure-related effects on lineprofiles. From Fig. 5c and d it is seen that the sensitivity of each turning point depends on its location from the linecenter, with the turning point farthest from the linecenter being most sensitive to the broadening. However, it is noted that in situation where absorption is weak, the turning points in the far-wing region will not be possible to discriminate because their magnitudes will be limited by the experimental SNR or the noise floor.

The plots showing effects of collision broadening in Fig. 5c were obtained by changing only the collision width to obtain a change in the b parameter of $\pm 10\%$; therefore, the Doppler width was kept constant and Eq. (5) was used to model the WMS-HHD signals. The plots showing the effects of Doppler broadening in Fig. 5d were obtained by only changing the Doppler width to obtain change in the b parameter of $\pm 10\%$, and the collision width was kept constant. Here, Eq. (5) was re-written to Eq. (7). This was done to redefine the modulation index and the normalized frequency in terms of the collision width, and to keep both of these parameters independent of the Doppler width. Therefore, when the Doppler width is changed it does not affect the effective modulation index, m of WMS-HHD models. Therefore, in Eq. (5) if the normalized frequency is re-defined as $xt \equiv xt/b = (v - v_0)/\delta v_L$.

Then Eq. (5) can now be re-written as

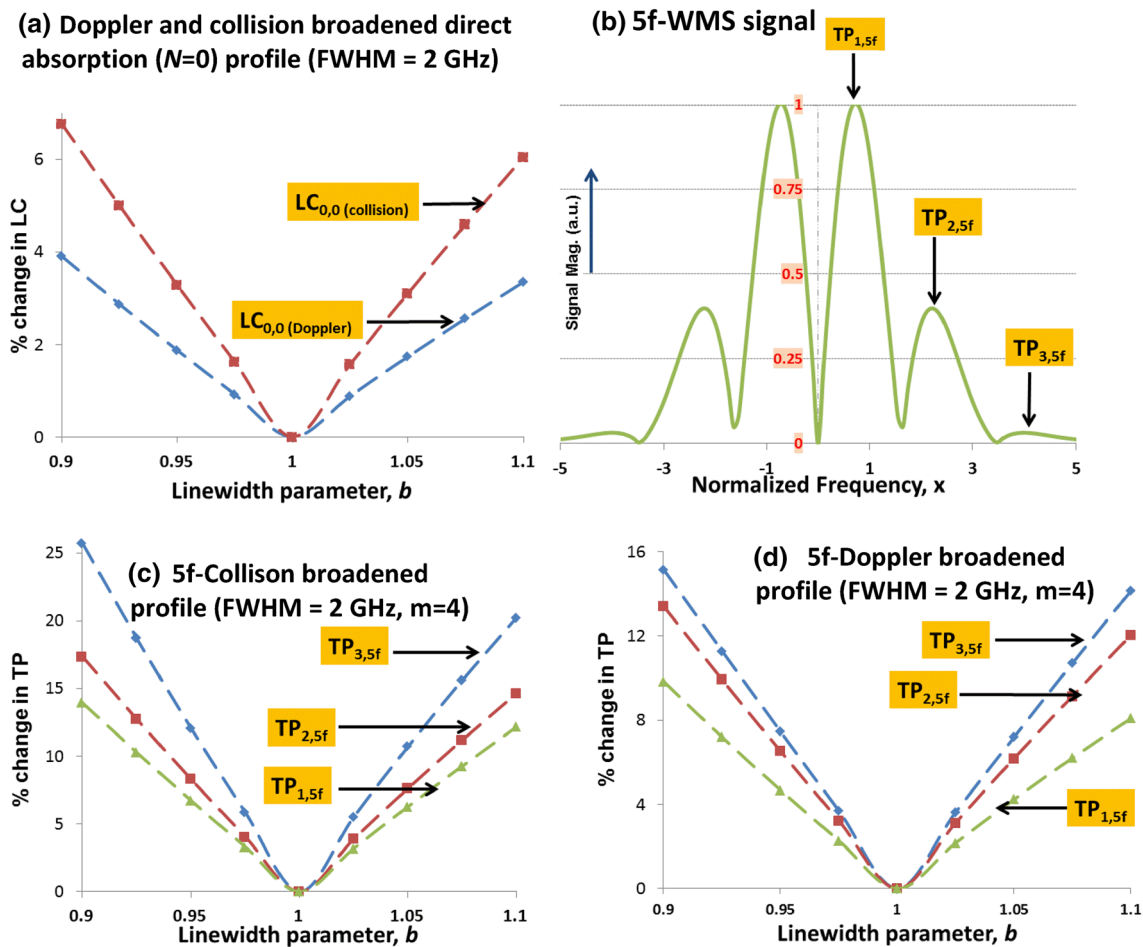


Fig. 5 Theoretical models showing variations of linecenter values of direct absorption, $N=0$ (a), and turning points ($TP_{i,Nf}$) of a collision- (c) and Doppler-broadened (d) 5f-WMS signal of atmospheric

oxygen $^{16}O_2$ -RR(13,13) line transitions. The turning point labels of a typical 5f-WMS signal are indicated in (b)

$$S^N(x') = \frac{I_0}{\pi} \int_{-\pi}^{\pi} d\theta \left[1 - \exp\left(\frac{n\bar{\sigma}L}{\pi^{3/2}\delta v_L} \int_{-\infty}^{\infty} dt \frac{e^{-t^2}}{(x' + m' \cos \theta - t/b)^2 + 1} \right) \right] \cos(N\theta) \quad (7)$$

Here frequency modulation index now becomes $m' = \beta/\delta v_L$.

It is noted that the sensitivity of the signal at turning points and zero crossings is reduced at higher modulation index values. This is a result of modulation broadening of the signal [12, 19]. The locations of the zero crossings and turning points and their sensitivity depend considerably on the lineshape function and the probe modulation index (m). For example, if $m \geq 1$ (the modulation amplitude is of the order of, or greater, than the linewidth), the turning points (in wings) are less sensitive to changes in the linewidth for lower WMS detection orders, e.g., 2f. This is because the

first turning point occurs in the spectral range of a half-width, while the remaining turning points (and zero crossings) appear in the wings. Since, the Doppler-broadened lineshape function falls off rapidly in the wings, the corresponding WMS signal manifests this feature in the wing structure—in their locations and sensitivity of the turning points. In contrast, if the profile is collision broadened, i.e., it has a sharper peak and falls off much more slowly in the pedestals, then the turning points in the wing region will be relatively more sensitive compared to those in a Doppler-broadened profile.

3.2 Broadening effects on signal structure of WMS-HHD

The previous analysis described in Sect. 3.1 was extended to investigate the behavior of various WMS-HHD signals on broadening mechanisms. It is seen that the profile broadening effect on turning points are also evident in higher detection orders. Figure 6a and b shows a comparison of

the linecenter (indicated as “ $LC_{0,Direct}$ ” in Fig. 6, which is the turning point of the direct absorption signal) and turning points of 2f-, 4f- and 6f-WMS signals of collision broadened, Fig. 6a, and Doppler broadened, Fig. 6b, profiles. It is seen higher detection orders have turning points more sensitive to changes in the b parameter than lower detection orders. In addition, collision-broadened profiles are more sensitive than the Doppler-broadened profiles; this is consistent with results obtained in the previous section. This is also central in demonstrating the utility of WMS-HHD as higher detection order has a greater number of such turning points (and zero crossings) available in the wing region. This can be used for an accurate estimation of profile parameters or characterizing signal broadening effects under a set of specific environmental conditions.

3.3 Experimental demonstration of WMS-HHD signals due to collision broadening

The sensitivity trends of turning points of WMS-HHD signals was corroborated with experiments probing oxygen RR(13,13) line transitions. Here the pressure of the enclosed gas (at room temperature) was changed to investigate the sensitivity of the turning points of WMS-HHD signals. To

illustrate our point, we recorded various turning points of various (2f to 6f) WMS-HHD signals, as shown in Fig. 7. The fractional change in each i th turning point ($TP_{i,Nf}$) of WMS-Nf detection order at reduced pressure was normalized to turning points at an atmospheric pressure of 760 torr. In Fig. 7, the 6f detection order shows higher sensitivity to pressure than 2f and 4f. Also, turning points in wing region of a particular WMS detection order also show greater sensitivity. Therefore, within the limits of the experimental SNR, turning points in the wing region tend to be more sensitive, i.e., the second turning point of 4f and first turning point of 6f is more sensitive to their respective linecenter values. The increase in sensitivity of turning points due to pressure is largely attributed to lineshape broadening and dominance of collision broadened effects at higher pressures.

From the theoretical and experimental analysis discussed in this section it is concluded that variations in turning points reveal critical information of the gas dynamics and environmental conditions. In a real scenario, such variations will be manifested in changes in both the temperature and pressure. The behavior of turning points and their combinations can be used for a fast determination of gas dynamics [28, 29] and provide a more robust and accurate characterization of the lineshape profiles and gas concentration levels.

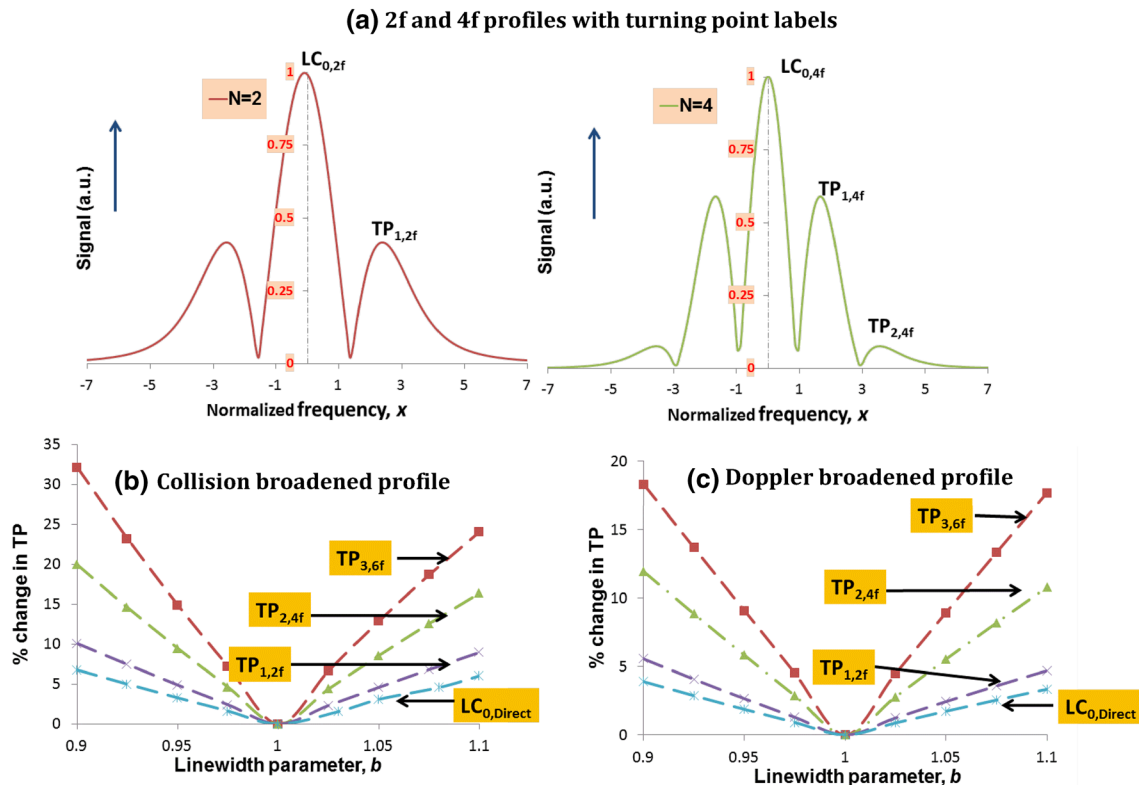


Fig. 6 Theoretical models showing variations of first, second and third turning point ($TP_{i,Nf}$) of a 2f-, 4f- and 6f-collision- (a) and Doppler-broadened (b) WMS-HHD profiles of $^{16}O_2$ -RR(13,13) line trans-

sitions. The models are compared with variation of linecenter values (indicated as “ $LC_{0,Direct}$ ” in a and b) of respective collision- and Doppler-broadened direct absorption signals

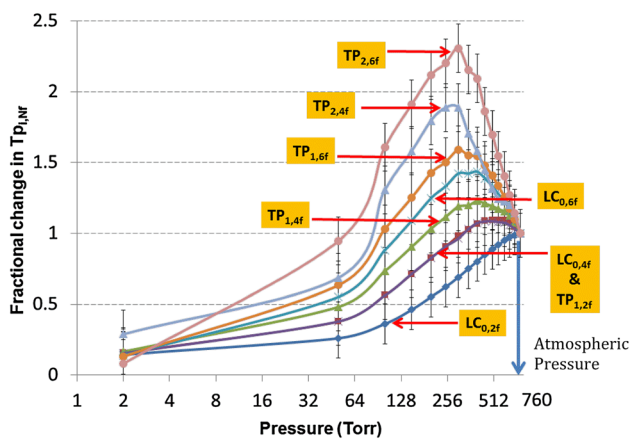


Fig. 7 Turning points of experimental WMS-HHD of $^{16}\text{O}_2$ -RR(13,13) line transitions at various pressures, plotted on a logarithmic scale. The plot shows sensitivity of linecenter, first and second turning points of 2f, 4f, and 6f WMS-HHD signals. The notation $\text{TP}_{i,Nf}$ indicates i th turning point of Nf detection order, and $\text{LC}_{0,Nf}$ indicates linecenter magnitude of Nf detection order

4 Detection of oxygen isotopes ($^{16}\text{O}^{18}\text{O}$) in enhanced WMS-HHD structure

In this section we show a direct application of structure in WMS-HHD in the detection of weaker line transitions. This improved signal contrast, and a direct consequence of resolution enhancement in higher WMS-HHD signals, is demonstrated in experiments showing amplification of weaker isotopic transitions with an atmospheric abundance of 0.4%. These isotopic transitions of $^{16}\text{O}^{18}\text{O}$ —RR(13,13), and RQ(12,13)—are in the wing region of the stronger $^{16}\text{O}_2$ -RR (13,13) line transitions (atmospheric abundance of 99.5%), shown in Fig. 8. The strong $^{16}\text{O}_2$ -RR (13, 13) transitions are centered at 760.378 nm ($13151.34863\text{ cm}^{-1}$) with linestrength of $5.68 \times 10^{-24}\text{ cm}^2\text{ molecule}^{-1}\text{ cm}^{-1}$. The neighboring weaker lines of $^{16}\text{O}^{18}\text{O}$ isotopic transitions—RR (13,13) and RQ (12,13)—are centered at 760.355 nm ($13151.73588\text{ cm}^{-1}$), and 760.317 nm ($13152.3997\text{ cm}^{-1}$) with line strengths of $1.12 \times 10^{-26}\text{ cm}^2\text{ molecule}^{-1}\text{ cm}^{-1}$, and $1.38 \times 10^{-26}\text{ cm}^2\text{ molecule}^{-1}\text{ cm}^{-1}$ according to the HITRAN 2017 database [21].

As mentioned previously, the signal sensitivity is directly related to the signal contrast with the background or its structure. The optimization of the signal structural can be achieved by selecting appropriate modulation indices and WMS detection orders, such that the overlap between lines is minimal, and the SNR of WMS signal corresponding to each transition is optimal. In other words, the experimental control parameters are selected in a manner that spectral locations and signal magnitudes of turning points and zero crossings are distinct, which leads to an enhancement of subtle features in a WMS-signal. This is demonstrated by

the amplification of weaker isotopic lines of $^{16}\text{O}^{18}\text{O}$ molecular transitions using WMS-HHD, where 6f or 7f detection shown in Fig. 8a and b has a greater signal contrast than the 2f-WMS signal shown in Fig. 8c. In Fig. 8d the 2f, 6f and 7f signals of isotopic transitions were analyzed by normalizing the Nf signal of strong $^{16}\text{O}_2$ RR (13,13) transition to unity. It is notable that we see relative amplification of Nf signals of weaker isotopic transitions (with respect to stronger transition) demonstrating strength of WMS-HHD technique.

The experiments in Fig. 8 were conducted with pathlength of 140 m in open air. The peak fractional absorbance in the pathlength of 140 m are: 0.91 for the stronger $^{16}\text{O}_2$ RR(13,13) transition, 3.14×10^{-6} for the isotopic $^{16}\text{O}^{18}\text{O}$ RR(13,13) transition, 5.9×10^{-6} for $^{16}\text{O}_2$ RR(43,43) transition and 3.12×10^{-6} for the isotopic $^{16}\text{O}^{18}\text{O}$ RR(12,13) transition. In addition, the frequency modulation index was $m = 8$ (based on the Doppler width of the strong $^{16}\text{O}_2$ RR(13,13) transition). The index value was chosen mainly to avoid overmodulation and overlap of Nf signals of the strong $^{16}\text{O}_2$ transition and enhance Nf signals of weaker transitions in the wing region. Another key point to note is that due to the differences in mass of abundant oxygen and isotopic oxygen, the Doppler width of $^{16}\text{O}^{18}\text{O}$ isotopic transitions (HWHM Doppler = 0.32 GHz) is smaller than that of strong $^{16}\text{O}_2$ transition (HWHM Doppler = 0.47 GHz). This results in relatively higher modulation indices, which combined with the effect of greater number of zero crossings and turning points (or the WMS structure) results in the relative amplification of Nf signals of weaker isotopic transitions.

To study the WMS-HHD signal structure and its relation with the experimental optical depth, experiments were performed by varying the sample pathlength. As mentioned earlier, the turning points and zero crossings embody the structure of WMS signals. Their signal magnitudes and spectral locations are representative of line parameters and experimental conditions, e.g., the optical depth in this particular case. From our analysis we see that under a specific set of optical depths, there are situations when variations in the signal in the wing region may be prominent, even though the total signal power may not show appreciable change, and, in some cases, it may even decrease. The aspect of structure and effective growth of signal in the wing region is shown as variation of turning points with the sample pathlength and the optical depth. To compare the growth of the signal in the wing region, individual turning points of WMS-HHD signal were normalized to the linecenter values. Therefore, this normalized ratio $R_T (= \text{TP}_{i,Nf}/\text{LC}_{0,Nf}$, where $\text{TP}_{i,Nf}$ is the i th turning point from the linecenter $\text{LC}_{0,Nf}$ of the Nf signal) provides a quantitative measure of the signal contrast with the background. In cases when R_T shows positive growth, i.e., turning points are amplified with respect to the linecenter magnitude; this indicates an improvement in signal contrast.

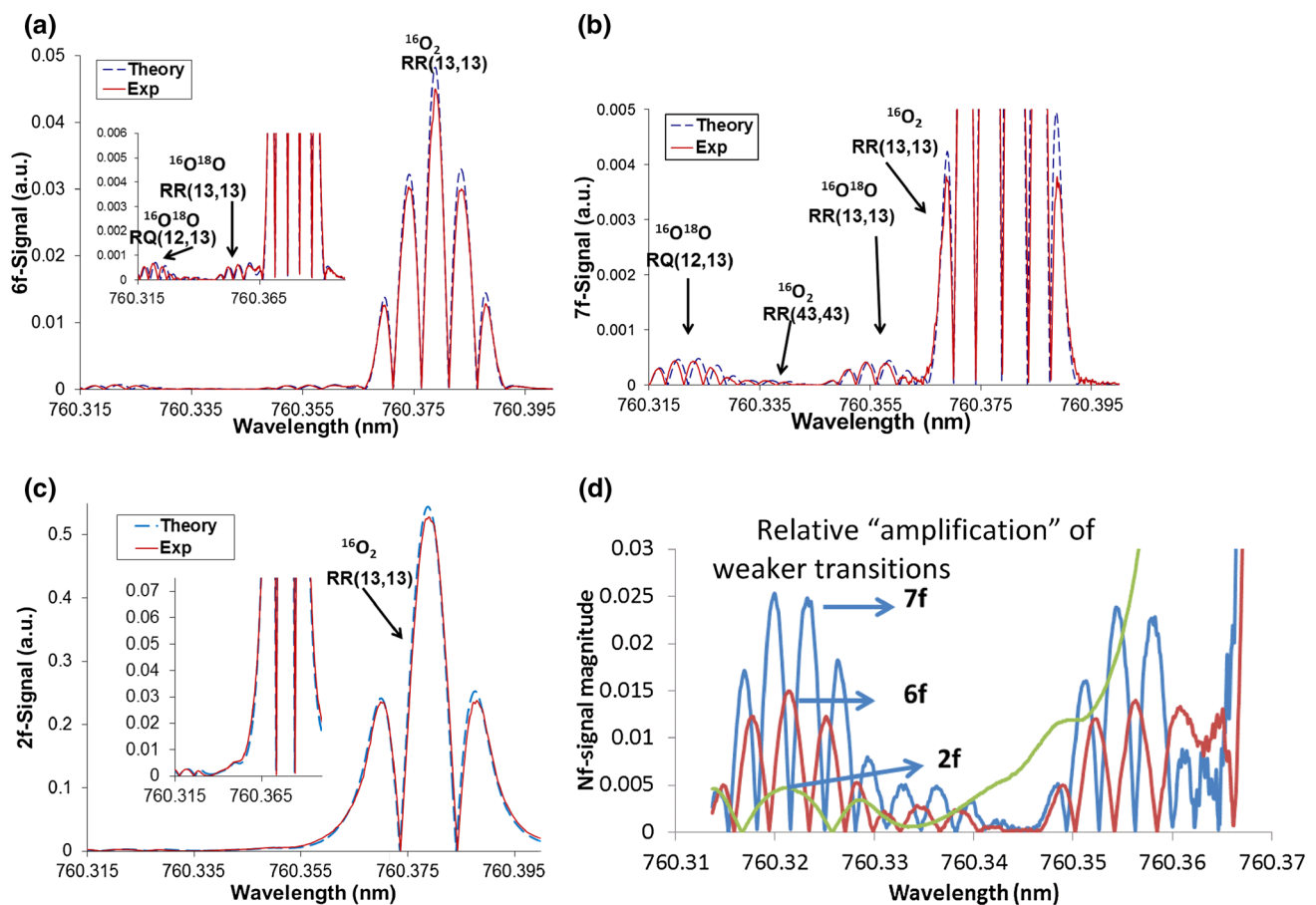


Fig. 8 Experimental 6f- (a), 7f- (b) and 2f- (c), WMS-HHD signals of atmospheric $^{16}\text{O}_2$ A-band transitions at 760 nm. WMS signals, particularly the ones higher than 6f begin to show weaker isotopic $^{16}\text{O}^{18}\text{O}$ transitions. In **d**, the peak values of 2f-, 6f-, and 7f-WMS

signal of the neighboring strong RR(13,13) transition of $^{16}\text{O}_2$ are normalized to unity, which shows growth of 7f and 6f signals from weaker transitions with respect to stronger $^{16}\text{O}_2$ transition

In Fig. 9, we show the characteristic behavior of the ratio R_T of even-harmonics of WMS-HHD signals with the sample pathlength or the optical depth ($\alpha = n\bar{\sigma}Lg(\nu_0)$). In a measurement where density (n), absorption cross section ($\bar{\sigma}$), and the lineprofile ($g(\nu)$) are fixed, the optical depth (α) can be varied by the pathlength (L) that the laser beam traverses in the absorbing medium. This was achieved by increasing the number of passes the laser beam makes between the mirrors of the multipass cell. In situations when the optical depth is large, i.e., $\alpha \gg 1$, there is a strong absorption or absorption saturation of the incident light. Figure 9a shows the ratio, R_T , of turning points of 8f-WMS signal of optically saturated RR(13,13) transitions of $^{16}\text{O}_2$. It is noted that at these high values of optical depth the linecenter values effectively remain unchanged with the pathlength. Therefore, the normalization of turning points with the linecenter has little effect on ratios, R_T , as the pathlength is increased. It is seen that there are certain regions in the wing where there is a net effective growth in the signal, indicated by an increase in R_T , Fig. 9a. The knee region in Fig. 9a shows the onset of strong saturation. This region is

more exaggerated in the turning points, $\text{TP}_{1,8f}$ and $\text{TP}_{2,8f}$ closest to the linecenter, whereas the turning point $\text{TP}_{3,8f}$, which is the farthest from the linecenter, is least affected by saturation effects. Therefore, it can be postulated that this region ($\text{TP}_{3,8f}$), which is relatively unperturbed, can be useful in investigating subtle lineshape deviations, e.g., profile narrowing effects or asymmetries in the lineshape profile from interfering isotopic transitions. The neighboring weaker lines, especially RR(13,13) transition of isotopic $^{16}\text{O}^{18}\text{O}$ begins to grow with higher WMS-HHD as the pathlength is increased and causes significant overlap with turning points in the farthest wing of the strong RR(13,13) line. Therefore, the fourth turning point of 8f detection is indiscernible and not shown in Fig. 9a. The above-mentioned increase in the signal in the wing region is also true for detection at other harmonics as seen in Fig. 9b. Here, even though the total signal power decreases with the increase in detection order, the wing region of 8f-WMS detection still seems to be most sensitive to the optical pathlength.

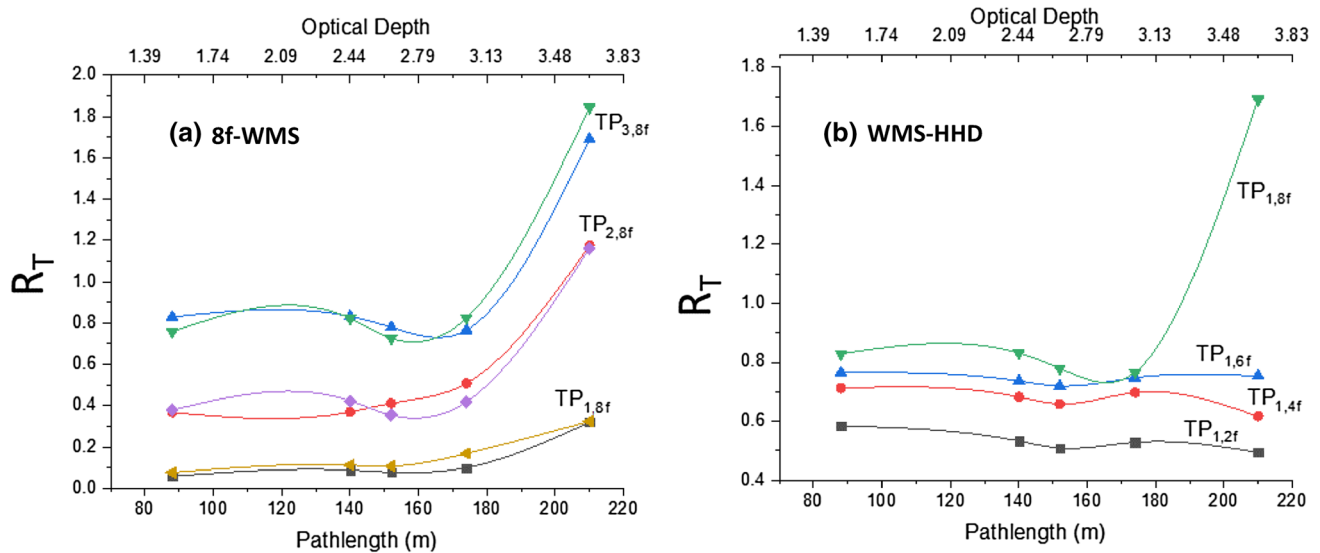


Fig. 9 Experimental values of ratios $R_T (=TP_{i,Nf}/LC_{0,Nf})$ of first, second and third turning points of 8f-WMS signal (a) and comparison of R_T of 2f- to 8f-WMS-HHD (b) RR(13,13) transitions of atmospheric

$^{16}\text{O}_2$. The two overlapping curves in a corresponding to $TP_{i,Nf}$ denote turning points on both sides of the linecenter, which can be used to investigate lineshape symmetries

5 Conclusions

The method discussed in this work provides a novel technique to quantify WMS-HHD signal structure useful for many laser-based sensing applications. The technique can be employed to study fluctuations in the lineshape parameters due to changes in the environment and molecular collision dynamics. The techniques for probing features of spectral profile encoded in turning points or zero crossings of WMS-HHD signals can be used for robust calibration schemes and monitor sensor performance under field conditions. In addition, this can also provide a useful metric to study and characterize lineshape features and molecular collision dynamics. Therefore, the method can be extended to investigate line-wing structure using combinatory ratios of turning points of WMS-HHD. Finally, since the method effectively utilizes probe of derivative-like features of the lineshape function, an appropriate WMS detection order (Nf) can be selected for high-precision measurements based on the required application. For example, the technique can detect variations in the wings that are not discernible or suppressed in direct absorption or lower order WMS signals. This could, among other things more accurately detect subtle features, e.g., deviations from Voigt profiles [30] or narrowing effects [31] of the spectral lineshapes such as Dicke narrowing.

Acknowledgements We acknowledge support from NSF-CREST—HRD1242067 and NSF Award 1645287. Richard Garner was supported by NSF-CREST award from the National Science Foundation. We also acknowledge support from NASA-MIRO Award NNX15AP84A

and NIH-INBRE (NIGMS-8 P20GM103446-16), Delaware State Supplement.

References

1. T.G. Edward, A.L. Donald, *Appl. Phys. Lett.* **8**, 227 (1966)
2. A. Siegman, *Lasers* (University Science Books, California, 1986), pp 167–171. ISBN-13: 978-0935702118
3. J.A. Aguilera, C. Aragon, *Spectrochim. Acta Part B* **63**(9), 893 (2008)
4. R.H. Dicke et al., *Phys. Rev.* **70**(6), 340 (1946)
5. L. Tao, K. Sun, M.A. Khan, D.J. Miller, M.A. Zondlo, *Opt. Express* **20**(27), 28106–28118 (2012)
6. D.J. Miller, K. Sun, L. Tao, M.A. Khan, M.A. Zondlo, *Atmos. Meas. Tech.* **7**, 81 (2014)
7. L. Tao, K. Sun, D.J. Miller, D. Pan, L. Golston, M.A. Zondlo, *Appl. Phys. B*, **119**(1), 153–164 (2015)
8. J. Reid, D. Labrie, *Appl. Phys. B* **26**, 203 (1981)
9. D.T. Cassidy, J. Reid, *App. Opt.* **21**, 7 (1982)
10. J.A. Silver, *Appl. Opt.* **31**, 707 (1992)
11. P.L. Varghese, R.K. Hanson, *Appl. Opt.* **23**(14), 2376 (1984)
12. A.N. Dharamsi, *J. Phys D Appl. Phys.* **29**, 3 (1995)
13. A.N. Dharamsi, A.M. Bullock, *Appl. Phys. Lett.* **69**, 22 (1996)
14. K. Mohan, M.A. Khan, A.N. Dharamsi, *Appl. Phys. B* **102**(3), 569–578 (2011)
15. P. Kluczynski, J. Gustafsson, A.M. Lindberg, O. Axner, *Spectrochim. Acta B* **56**, 1277 (2001)
16. C.S. Goldenstein, C.L. Strand, I.A. Schultz, K. Sun, J.B. Jeffries, R.K. Hanson, *Appl. Opt.* **53**, 356–367 (2014)
17. K. Sun, X. Chao, R. Sur, C.S. Goldenstein, J.B. Jeffries, R.K. Hanson, *Meas. Sci. Technol.* **24**, 125203 (2013)
18. J. Altman, R. Baumgart, C. Weitkamp, *Appl. Opt.* **20**, 995 (1981)
19. G.V.H. Wilson, *J. Appl. Phys.* **34**, 3276 (1963)
20. O.E. Meyers, E.J. Putzer, *J. Appl. Phys.* **30**, 1987 (1965)

21. I.E. Gordon, L.S. Rothman et al. *J. Quant. Spec. Rad. Tran.* **203**, 3–69 (2017)
22. M.A. Khan, J.M. Barrington, A.N. Dharamsi, *Proc. SPIE* **4634**, 83–91 (2002)
23. A.N. Dharamsi, Y. Lu, *Appl. Phys. B* **62**, 273 (1996)
24. A.N. Dharamsi, Y. Lu, *Appl. Phys. Lett.* **65**, 2257 (1994)
25. A.N. Dharamsi, A.M. Bullock, *App. Phys. B* **63**(3), 283 (1996)
26. M. Amir Khan, K. Mohan, A.N. Dharamsi, *Appl. Phys. B* **99**(1), 363–369 (2010)
27. K. Sun, L. Tao, D.J. Miller, M.A. Khan, M.A. Zondlo, *Appl. Phys. B* **110**(2), 213–222 (2013)
28. A. Farooq, J.B. Jeffries, R.K. Hanson, *Appl. Phys. B* **96**(1), 161–173 (2009)
29. X. Chao, J.B. Jeffries, R.K. Hanson, *Appl. Phys. B* **106**(4), 987–997 (2012)
30. J. Ward, J. Cooper, *J. Quant. Spec. Rad. Tran.* **14**, 555 (1974)
31. R.H. Dicke, *Phys. Rev.* **89**(2), 472 (1953)